# Wing LCO at Transitional Re Numbers

**Dominique Poirel**
Department of Mechanical Engineering
Royal Military College of Canada
PO Box 17000, Stn Forces
Kingston, Ontario, Canada, K7K7B4
(currently on sabbatical at NRC/IAR, Ottawa, Canada)

E-mail: poirel-d@rmc.ca

## *ABSTRACT*

*Experimental observations of self-excited, small amplitude, pitch oscillations of a rigid, but flexibly mounted, NACA 0012 airfoil at transitional Reynolds numbers were recently reported. The LCOs occur in the range 5.0 $\times 10^4 \leq Re_c \leq 1.3 \times 10^5$. They are well-behaved, have a small amplitude ($\pm \sim 5°$) and oscillate about $\theta = 0°$. It has been speculated that the complexity of the viscous phenomena, such as laminar separation leading to the formation of a LSB, occurring at these Reynolds numbers plays an essential role in these oscillations. Accordingly, they are reminiscent of stall flutter except that they occur at very low angles of attack and are strongly Re dependent. Flow visualization techniques applied to the statically held airfoil at these Reynolds numbers and angles of attack confirmed the existence of these viscous phenomena. For the free pitching airfoil, considering that the experimental rig acts as a dynamic balance, the aerodynamic moment is derived using the Restoring Force Surface method in conjunction with a least-square surface fit procedure. As expected, it behaves nonlinearly with pitch displacement and velocity. An empirical model of the aerodynamic moment, in the sense of a generalized Duffing-van der Pol nonlinearity, is proposed.*

## 1.0 INTRODUCTION

Limit cycle oscillations (LCO), being a nonlinear phenomenon, requires the existence of at least one nonlinear element in a given system to occur. For an aeroelastic system, the nonlinearity may be structural, aerodynamic or both. From an aerodynamic point of view, classical observations and subsequent investigations on wings have focused almost exclusively on the following two nonlinear flow regimes: transonic and high angle-of-attack. The former is often experienced on high performance aircraft; its physical mechanism is intimately tied to the presence and motion along the wing surface of a shock wave whose one important feature is a sharp increase in pressure. In the other regime, at high angle-of-attack (AOA), flow separation is the physical cause of the nonlinearity. It is observed on the retreating blade of a helicopter rotor, for instance. This flow separation may lead to stall flutter.

Recent wind tunnel observations of a free pitching NACA0012 wing experiencing small amplitude self-sustained oscillations in the so-called low Re regime, or more precisely the transitional regime, have extended the domain in which aerodynamic nonlinearities have a profound impact on aeroelastic stability [1]. This comes to no surprise since the flow at $10^4 < Re_c < 10^6$ is highly nonlinear; complex viscous phenomena occur

such as laminar boundary layer separation, transition of the laminar shear layer and subsequent re-attachment of the turbulent layer thus leading to the time-averaged formation of a laminar separation bubble (LSB) [2,3]. The consequence of these viscous events on the aerodynamic loads is such that the static lift curve, for instance, is a nonlinear function of the angle of attack even well below stall [4,5,6]. The change of slope ($C_{L\alpha}$) at small angles of attack is associated with laminar trailing edge separation and the LSB. Similar trends have been observed for the aerodynamic moment [5,6]. For instance, see Fig. 1 which shows the static moment coefficient of a NACA0012 wing taken about the quarter-chord point for two Re numbers. These moments are reproduced from Huang *et al.* [6]. Note that moment coefficients actually published in [6] are an order of magnitude too large; this error was confirmed via email (2006). Surface-oil flow analysis indicated laminar separation from 0° to 2° followed by a LSB between 2° and 13° approximately [7]. Turbulent trailing edge separation occurring aft of the LSB for angles above 8° was also observed.

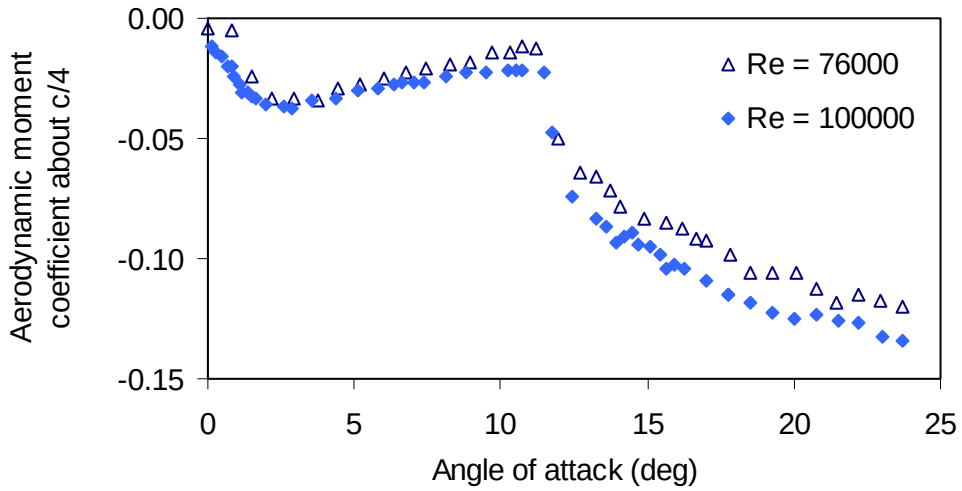


Figure 1 – Static aerodynamic moment coefficient about the quarter-chord.
NACA0012 wing with one end plate, AR = 5. Tu ~ 0.2%.
Reproduced in part from [6], Fig. 12.

In this paper, some important characteristics of the self-sustained oscillations observed in the Royal Military College of Canada's wind tunnel at these low Re numbers are described. Flow visualizations of the surface flow for the statically held airfoil in the same wind tunnel but using a different rig are then shown. This is followed by an analysis of the aerodynamic moment in these dynamic conditions, whereby the effects of low Re aerodynamics are discussed. An empirical model, in the sense of a generalized Duffing-van der Pol nonlinearity, is proposed.

## 2.0 EXPERIMENTAL OBSERVATIONS

### 2.1 Experimental Set-up

The wind tunnel used for these experiments and shown at Fig. 2 is a closed circuit. It can produce flow speeds ranging from 5 to 60 m/s. It has a test section of 0.76 m × 1.08 m and experiences a maximum turbulence intensity level less than 0.2% for the range of airspeeds considered in this work. The airspeed is measured with a pitot-static tube located at the inlet of the test section and linked to a manometer.

At the end of the test section, a two-degree-of-freedom (DOF) pitch-plunge apparatus system, composed of a rigid NACA 0012 wing moving in translation and in rotation is installed; see Fig. 3. The support structure, located outside the tunnel, has two similar top and bottom translating sub-systems, on which the rotation mechanisms are installed. Both rotation and translation mechanisms are comprised of two sets of pulley-spring to provide the elastic restoring force. The wing span is $s$ = 0.61 m and its chord is $c$ = 0.156 m, thus giving an aspect ratio, AR = 3.9. End plates are installed to minimize 3D effects. The gap between the wing tips and end plates is 7 mm, which is equivalent to 1% of the span. The wing and the end plates results in a solid blockage ratio of 5%. The axis of rotation (elastic axis, EA) of the wing can be modified; in its nominal configuration the EA is located 0.01 m forward of the quarter-chord point, i.e., at 18% chord aft of the leading edge. The mass ratio (based on the parts of the apparatus that rotate) is $\mu = m/(\rho\pi(c/2)^2 s) = 55.6$. The motion is measured with potentiometers and is sampled at 1000 Hz ($\Delta t$ = 0.001 s).

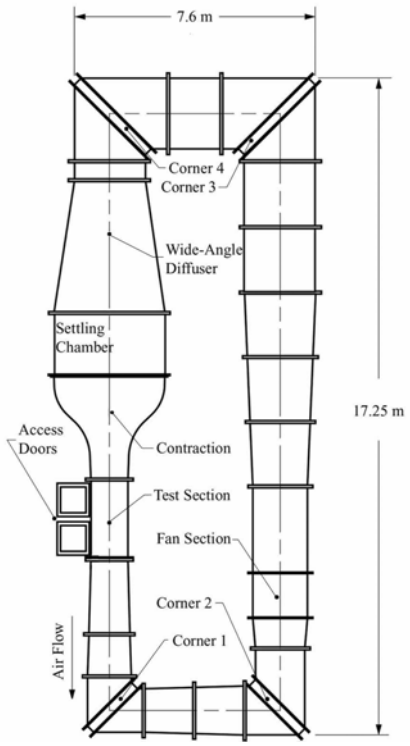


Figure 2 - The RMC low-speed wind tunnel.

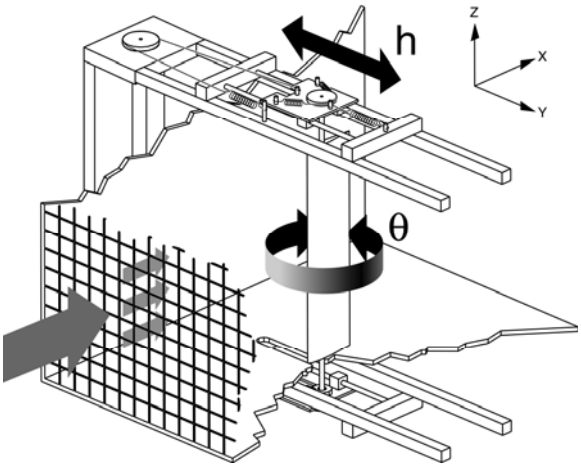


Figure 3 - Schematic of the aeroelastic apparatus.

## 2.2 Aeroelastic oscillations characteristics

The results illustrated in this paper are for the wing confined to pure rotation only; the plunge DOF is held fixed. In its nominal configuration, the wing has a mass moment of inertia about the EA, $Is$ = 0.00135 kg m$^2$, a structural stiffness coefficient, $Ks$ = 0.30 N m/rad, and a structural damping coefficient (assuming a linear viscous model), $Ds$ = 0.002 N m s. Additional details are provided in [1].

A typical time response is shown at Fig. 4, along with its phase plane representation. Note that the phase plane response is for the filtered data with a cut-off frequency, $f_c$ = 25 Hz; this is discussed in more details in Section

3. The time response reveals the loss of stability of the equilibrium point after a small perturbation, at approximately $t$ = 4 s, and re-stabilization on a limit cycle oscillation (LCO). These oscillations are self-sustained, or limit cycle, since there is no periodicity in the upstream flow, as measured with hot-wire anemometry, accounting for this behaviour, nor in its wake when the wing is held fixed. Should the pitch motion be caused by the aerodynamics acting as an external force, a periodicity in the flow corresponding to the pitch oscillations would be expected even if the wing is rigidly fixed. This is not the case.

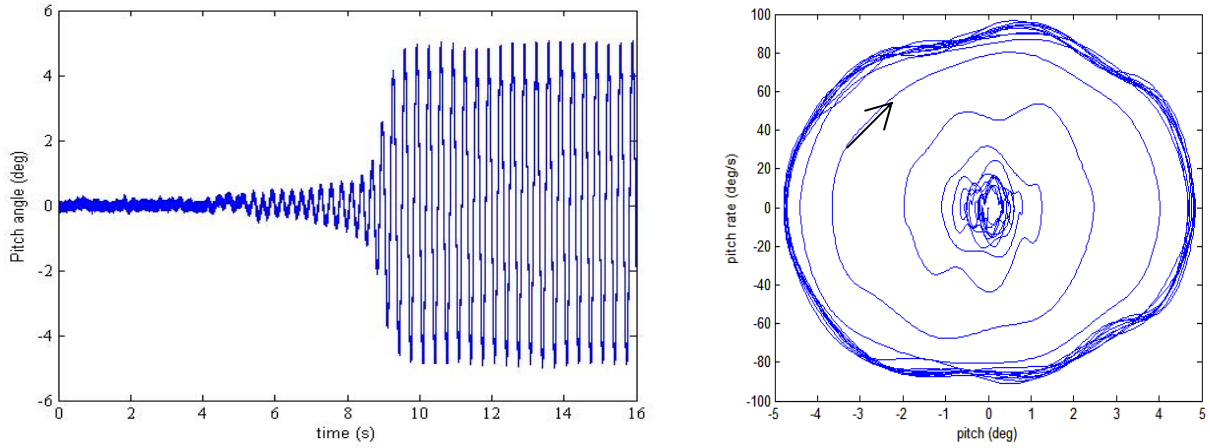


Figure 4 - Typical time response and (filtered) phase plane.
Nominal configuration ($K$s = 0.30, EA at 0.18$c$), $U$ = 7.5 m/s ($\mathrm{Re}_c$ = 77,000).

The oscillations exhibit essentially simple harmonic motion. Not shown but the spectral content of the pitch LCO dynamics displays a single dominant frequency, $f$, ($f$ = 2.9 Hz for the case illustrated in Fig. 4) as well as much weaker super-harmonics at 2$f$, 3$f$, 4$f$ and 5$f$. The even harmonics are due to a small misalignment between the wing chord and the in-coming freestream, whereas the odd harmonics are caused by inherent nonlinearities in the flow itself. No distinct dominating features are noticed at higher frequencies in the pitch response spectrum.

In the next two figures, the behaviour of the pitch oscillation amplitude and frequency with Reynolds number is plotted for various structural stiffness values and two positions of the elastic axis, one ahead and one slightly aft of the quarter-chord point. The LCOs occur for $\mathrm{Re}_c$ between approximately $5.0 \times 10^4$ and $1.3 \times 10^5$. Outside of this range, they are not sustained. The maximum oscillation amplitude happens for the case with no structural stiffness and is relatively small, below 6°. For the forward EA position at 0.18$c$, the oscillation frequency increases with airspeed. This is attributed to a positive aerodynamic stiffness which also increases with airspeed. At the zero airspeed (or $\mathrm{Re}_c$), the projection of the pitch frequency is the structure natural frequency. On the other hand, the aft EA position at 0.27$c$ indicates a slightly decreasing oscillation frequency, below the structural natural frequency, up to $\mathrm{Re}_c \approx 8.0 \times 10^4$ but which increases again for larger $\mathrm{Re}_c$. For the lower airspeed region, this behaviour is interpreted as being due to a negative aerodynamic stiffness. From the point of view of linear aerodynamics, the EA being aft of $c$/4, the wing is in divergence conditions. In this case, it is prevented from diverging by the structural stiffness. This is why the zero spring ($Ks$ = 0.0) case is not shown for this EA position. Furthermore, the fact that the frequency increases for the higher airspeed region indicates a strong Re dependency of the overall self-sustained oscillations, delimited by $\mathrm{Re}_c \approx 8.0 \times 10^4$.

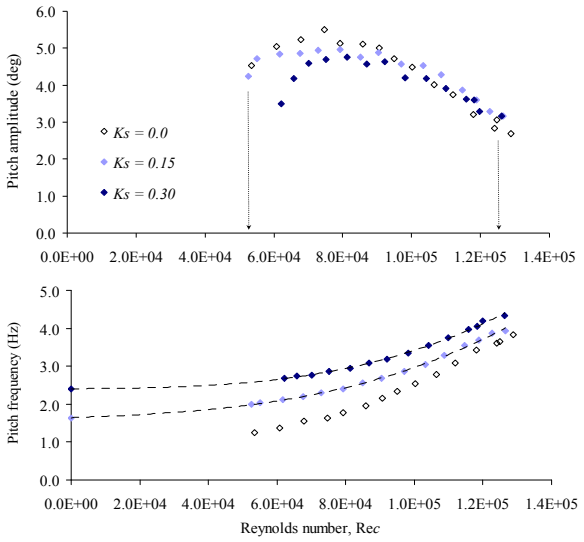


Figure 5 - Amplitude and frequency of oscillation for various stiffness coefficients. EA at 18% *c*.

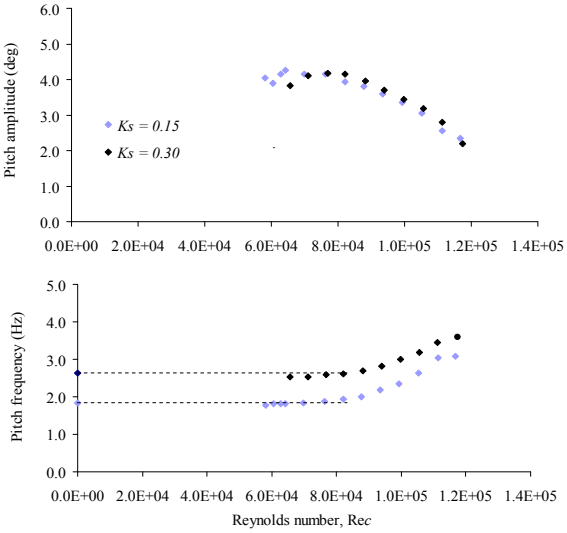


Figure 6 - Amplitude and frequency of oscillation for various stiffness coefficients. EA at 27% *c*.

This Reynolds number dependency is also illustrated from a slightly different perspective in terms of the reduced frequency as shown in the next figure. Two regimes of oscillations, under and above $Re_c \approx 8.0 \times 10^4$, are noticed.

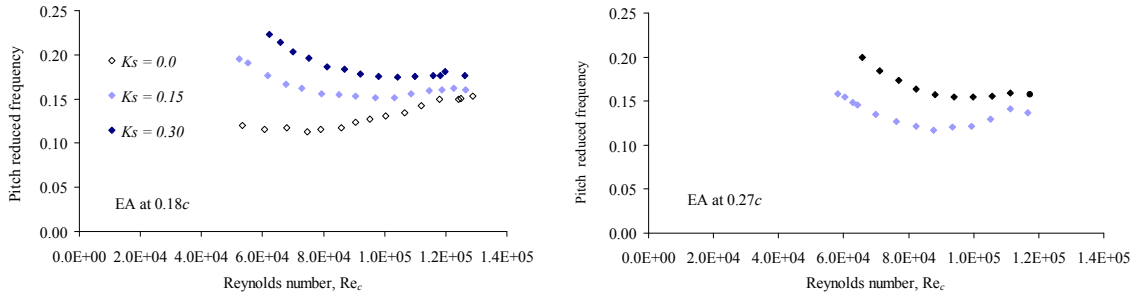


Figure 7 – Reduced frequency of the pitch oscillations for various stiffness coefficients and positions of elastic axis.

## 2.3 Flow visualization of the surface flow

In an effort to gain more insight into the behaviour of the boundary layer at these Reynolds numbers and angles of attack, additional tests were performed on a statically held NACA0012 airfoil. This was done in the same wind tunnel but using a different rig, shown in Fig. 8. The technique used was paraffin oil mixed with a fluorescent dye. Each test was run for 30 minutes in order to reach a stationary flow along the surface. Additional results and details are provided in [8].

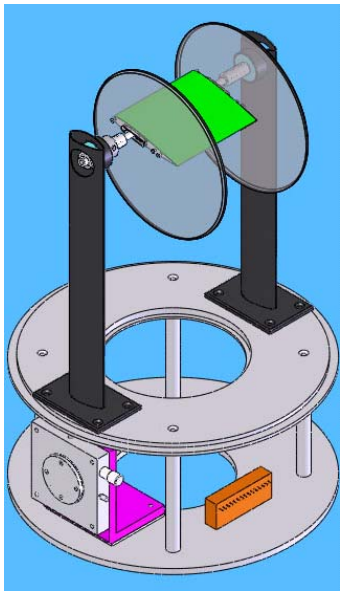

Figure 8 – Schematic of experimental rig for flow visualization

The next series of images show the results of these tests. Fig. 9 shows the behaviour as a function of Reynolds number for zero angle of attack. Laminar separation is clearly seen and travels aft with increasing $Re_c$. The boundary layer appears to re-attach close to the trailing edge at $Re_c$ = 77,000, thus creating a long LSB.

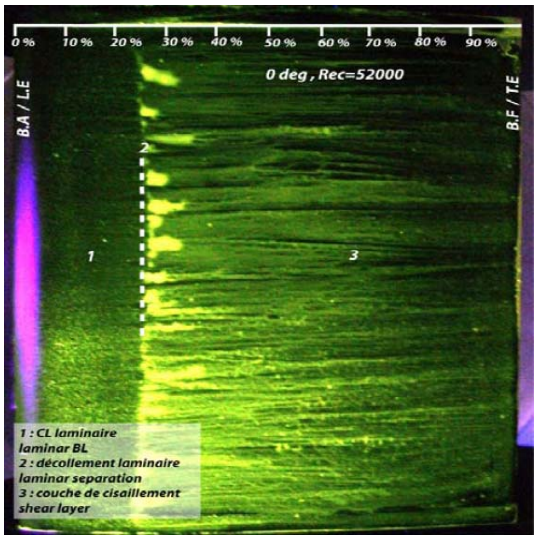


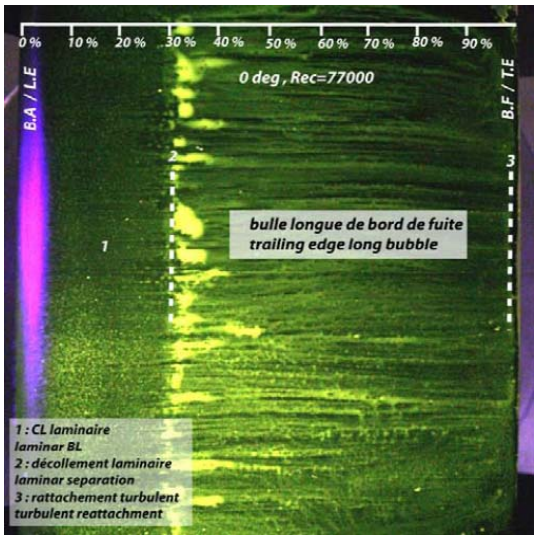

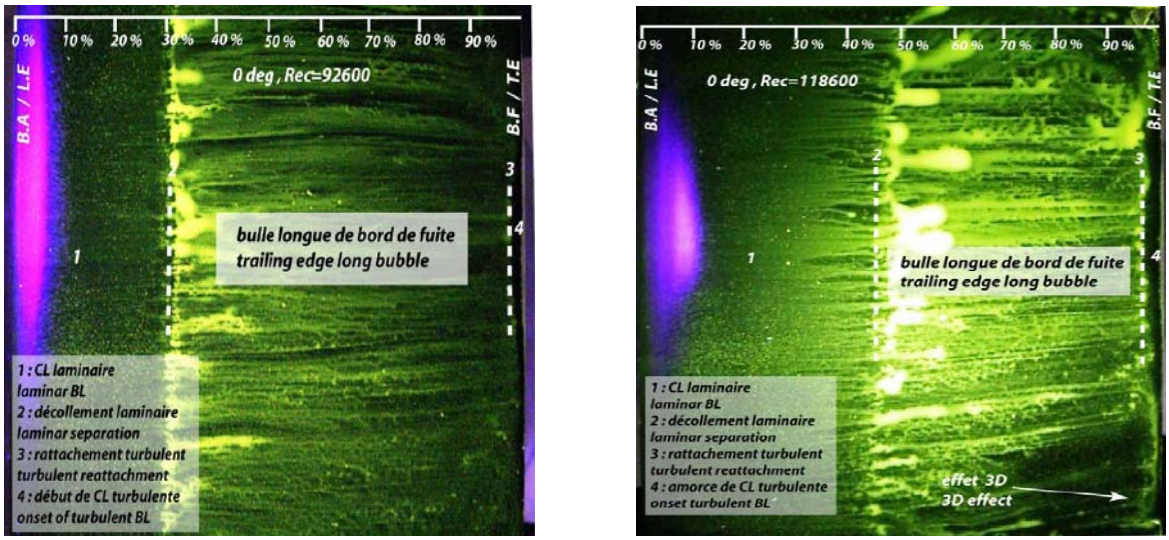


Figure 9 – Flow visualization as a function of $Re_c$ for $\alpha = 0º$.

For $Re_c$ = 77,000, the variations with angle of attack is shown in Fig. 10. The laminar separation point moves forward with angle of attack, similarly with the re-attachment point thus resulting in a decreasing size of the LSB. An additional feature appears at $\theta = 2º$ as the flow detaches again as a trailing edge turbulent separation.

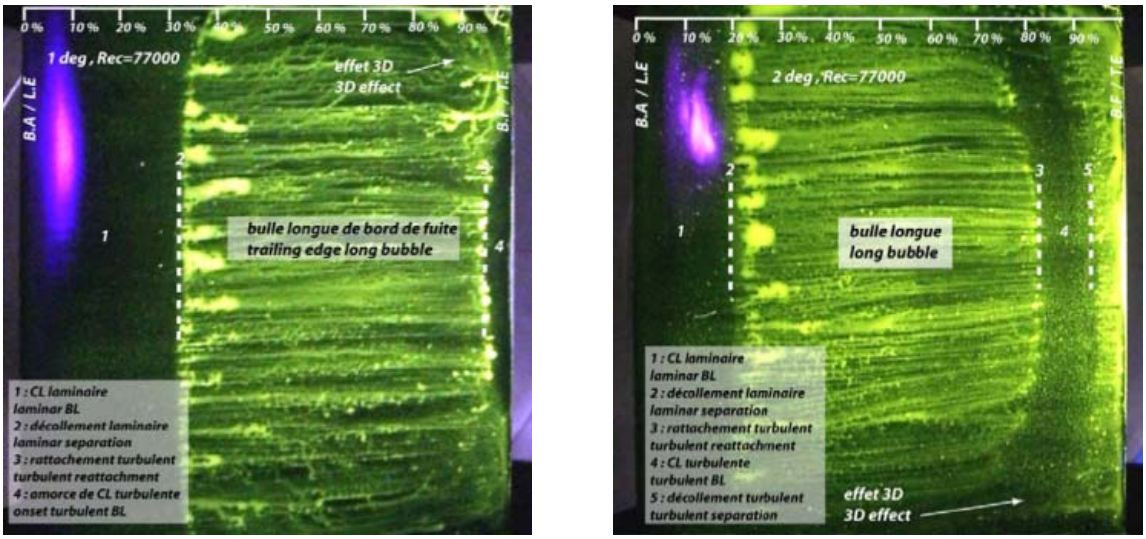

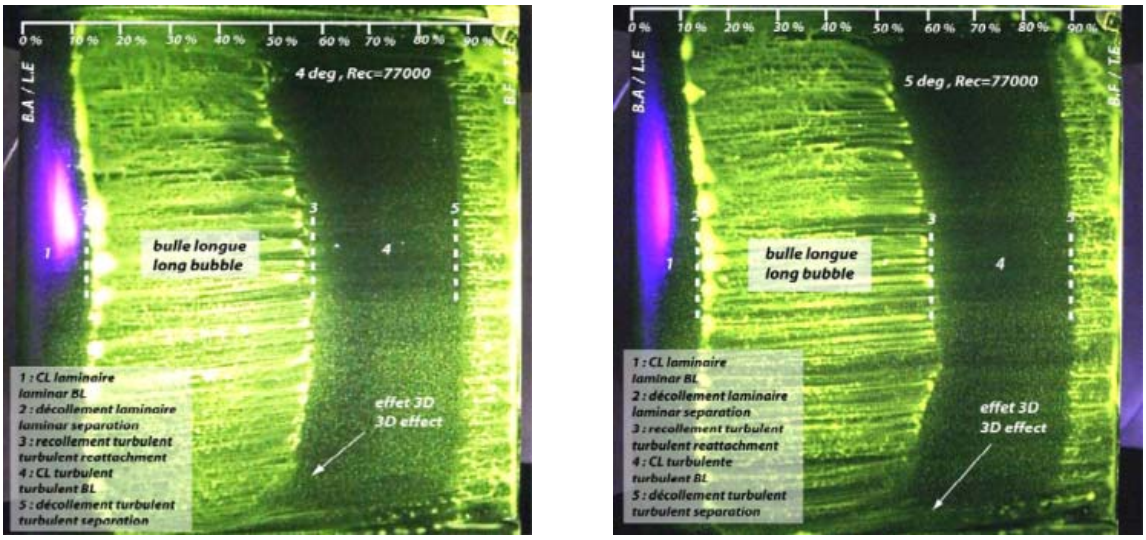


Figure 10 – Flow visualization as a function of $\theta$ for $Re_c$ = 77,000.

## 3.0 AERODYNAMIC MOMENT ANALYSIS

Considering that the flutter rig acts as a dynamic balance, the aerodynamic moment can be calculated from the recorded pitch motion and the measured rig structural properties simply from the following equation:

$$M_{EA} = I_s\ddot{\theta} + D_s\dot{\theta} + K_s\theta \tag{1}$$

The pitch rate and pitch acceleration are obtained by the first and second time derivatives, respectively, of the pitch time response. The numerical differentiation accentuates the high frequency noisy fluctuations present in the original signal, as well as the super-harmonics of the LCOs. Accordingly, the pitch response is first passed through a digital FIR filter with a cut-off frequency at 25 Hz followed by a very sharp drop in the gain; in this region from 0 to 25 Hz, the phase is linear which means that the phase of the super-harmonics is preserved as well. This cut-off frequency is high enough to pick up the super-harmonics of any significant strength, up to 7*f*, but low enough to neutralize the unwanted fluctuations which could be due to measurement noise or real physical processes such as turbulence or vortex shedding. The problem is that it is very difficult to differentiate between them, hence the prior filtering. Furthermore, as will be discussed later, it is believed that this self-sustained aeroelastic phenomenon is essentially dictated by low frequency physics such that the high frequencies can be neglected. The differentiation is performed using the five-point scheme described in [9]. It is shown in Eq. 2 for the pitch rate:

$$\dot{\theta}_i = \frac{1}{12\Delta t}\left(-\theta_{i+2} + 8\theta_{i+1} - 8\theta_{i-1} + \theta_{i-2}\right) \tag{2}$$

Once the pitch rate has been determined, the same procedure is the applied to get the pitch acceleration. A seven-point differentiation was also performed; negligible differences were noted for both the pitch rate and acceleration. The aerodynamic moment, normalized by $\frac{1}{2}\rho U^2 sc^2$, as a function of pitch angle is shown on Fig.

11 for the case presented in Fig. 4 and for $4.0 < t < 13.0$ seconds, and for two cut-off frequencies. The right hand plot is for a cut-off frequency just above the fundamental frequency of the LCO. It serves the purpose to more easily explain the dynamics at play. The same information, and more, is contained in the left hand plot. The important contribution of the super-harmonics is clearly visible. Looking at the right hand plot, the clockwise direction of the loop physically means that the work done by the airflow on the airfoil is positive. In other words, the aerodynamic damping is negative and the flow transfers energy to the structure and sustains the oscillations. Hence, they are self-sustained from an aeroelastic point of view.

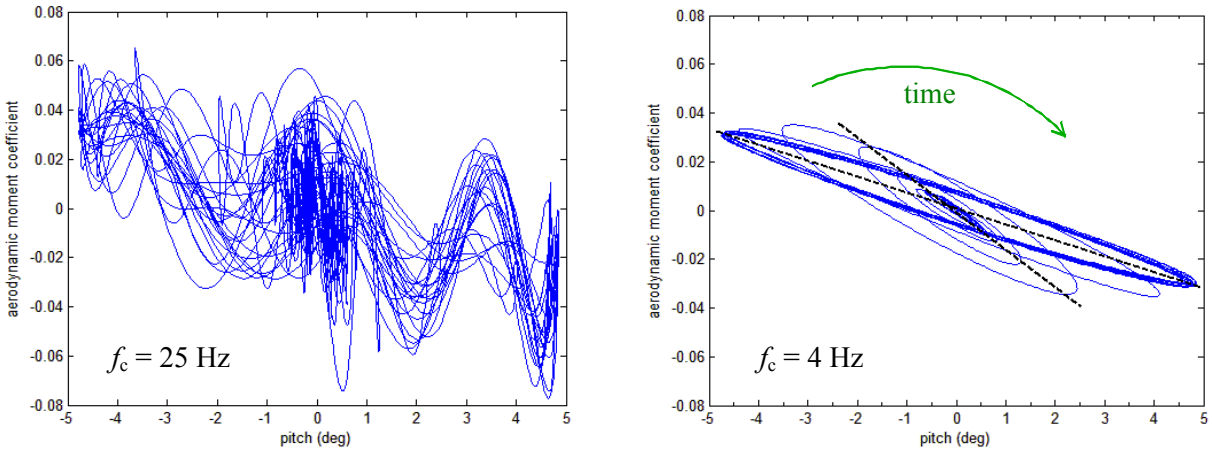


Figure 11 – Aerodynamic moment coefficient as a function of pitch angle, 4 s $\leq t \leq$ 13 s, for two different filter cut-off frequency. Nominal configuration ($K$s = 0.30, EA at 0.18$c$), $U$ = 7.5 m/s (Re$_c$ = 77,000).

The rotation of the main axis of the elliptical shape, as the oscillation amplitude grows with time until the dynamics reach the steady-state LCO, provides some indications about the aerodynamic torsional stiffness. The larger slope of the axis at small pitch angles compared with larger pitch angles means that the aerodynamic stiffness decreases with pitch angle. The change of stiffness with angle of attack can be physically related to the movement of the LSB, purely on the basis of static considerations. Taking into account that the LSB is a localized region where the flow is separated, it is associated with a pressure plateau at a lower value should it had remained attached. Past the re-attachment point, the pressure rises again. Furthermore, close to the leading edge the suction peak decreases to a larger pressure value due to the (local) separation. Assuming that the elastic axis is located between the suction peak and the LSB, the combination of the relative high pressure ahead of the EA and low pressure aft of the EA, respectively, causes a pitch down stabilizing moment, similar to high AOA stall. Looking at Fig. 10, the bubble which moves forward with angle of attack has less impact on the moment since its lever arm becomes smaller, hence the decreasing aerodynamic torsional stiffness.

### 3.1 Restoring force surface method

The application of the Restoring Force Surface method, in conjunction with a surface fitting procedure, provides a more rational framework to capture the aerodynamic moment characteristics. This system identification method has been applied with success to different problems and is particularly attractive for a SDOF system due to its simplicity. Details are provided in [9]. Applied to the current problem, the idea is the following. The aerodynamic moment, calculated from Eqs. 1 and 2 for a given time range is plotted on a 3D graph as a function of pitch displacement and pitch rate. Implicit to this formulation is the assumption that the aerodynamic moment is not an explicit function of the pitch acceleration and the time, hence:

$$M_{EA}(\theta,\dot{\theta},\ddot{\theta},t) \approx M_{EA}(\theta,\dot{\theta}) \tag{3}$$

This is in effect a quasi-steady approximation, and is justified by the following. The explicit pitch acceleration dependency represents the added mass of the fluid. It can be neglected on the basis of a large mass ratio, $\mu$ = 55.6, and a combination of a small pitch frequency and amplitude. The explicit time dependency reflects the effect of the shed vorticity in the wake caused by the pitching motion. Although its impact is felt upstream on the airfoil, each element of vorticity sees its effect diminishing in time as it is convected downstream with speed, $U$. Accordingly, the larger the airspeed $U$, the less effect it has. Inversely, the larger the pitching frequency the greater effect it has. This can be formally expressed by the reduced frequency. For linear aerodynamics, which is strictly speaking not the case here, the unsteady effects due to the shed vorticity can generally be neglected for $k < 0.05$. In this work, the pitch oscillation frequencies, in reduced form are in the order of 0.1 - 0.2; see Fig. 7. They are slightly higher than 0.05 but still of the same order of magnitude. To some degree, it is assumed that this linear aerodynamic limit can be generally applied to the nonlinear case. Furthermore, it is worthwhile to add that the experimentally observed pitch oscillations were not affected significantly by the presence of objects placed in the airfoil near wake. In particular, some tests were performed with a mesh installed in the wake of the wing, thus destroying any vortex shedding structure past this point, but with minimal impact on the aeroelastic LCOs. These considerations justify, to some extent, the quasi-steady approach.

A least-square surface fitting procedure is then applied to the experimentally derived aerodynamic moment. In this work a third-order polynomial is used in both states. It is in some sense a generalized Duffing-van der Pol type nonlinear model. It is given in Eq. 4.

$$M_{EA}(\theta,\dot{\theta}) = a_1 + a_2\theta + a_3\dot{\theta} + a_4\theta^2 + a_5\theta\dot{\theta} + a_6\dot{\theta}^2 + a_7\theta^3 + a_8\theta^2\dot{\theta} + a_9\theta\dot{\theta}^2 + a_{10}\dot{\theta}^3 \tag{4}$$

The result of the fit is shown in Fig. 12 for the normalized moment, $C_{\text{Mea}}$. Note that only the moment's values that correspond to the range of experimentally observed combinations of pitch angle-pitch rate are plotted. Looking down the moment coefficient axis on the pitch angle-pitch rate plane, the region covered is an image of the system state trajectories in the phase plane, as shown in Fig. 4 for the same case. Outside this range, the fit provides an extrapolation of the aerodynamic moment and is therefore considered not valid. The fitting procedure has obviously a smoothing effect on the moment. This is also seen in Fig. 11. In effect, the fitting eliminates the high frequency content of the aerodynamic moment. It enables a more focused perspective on the low frequency aerodynamics and is compatible with the quasi-steady model.

The aerodynamic moment is highly nonlinear in both angle and rate. This nonlinear behavior, even for small angles ($\theta \leq 5°$), is not surprising. It is a direct consequence of the complex flow physics occurring at transitional Reynolds numbers.

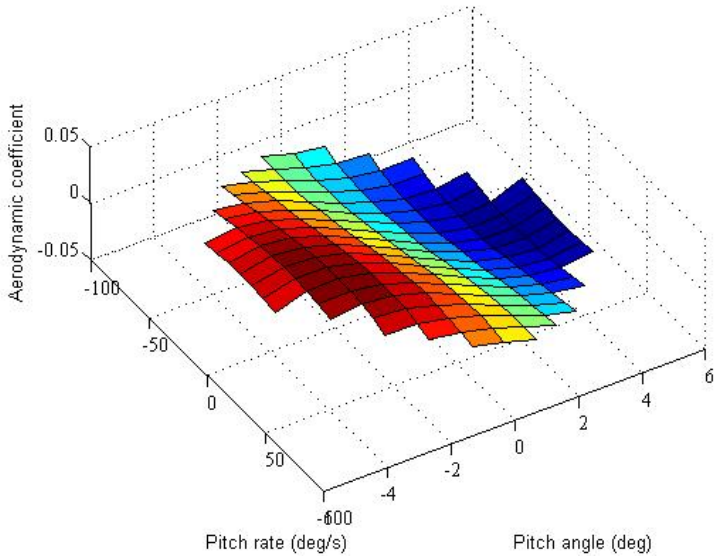


Figure 12 – Least-square fit of the aerodynamic moment coefficient as a function of pitch angle and pitch rate. Nominal configuration ($Ks$ = 0.30, EA at 0.18$c$), $U$ = 7.5 m/s ($\mathrm{Re}_c$ = 77,000).

Looking at the moment-angle plane for a zero pitch rate, the static case $C_{\mathrm{Mea}}(\theta)$ emerges and is reproduced in Fig. 13, left image. Also plotted for comparison is the linear thin airfoil theory model, as well as the experimental results from Huang *et al*. [6], also shown in Fig. 1. The agreement is very good but not perfect. This is expected due to some differences in the two configurations. Both are for a NACA0012 type airfoil at $\mathrm{Re}_c \approx 77{,}000$ and Tu ≈ 0.2%. The differences are in the axis about which the moment is calculated, 0.18$c$ for the current work and 0.25$c$ for Ref. [6], and in the wing configuration, free rotating wing with plates at both ends for the current work (ie. Q2D case) and a cantilevered wing with one end plate for Ref. [6] (ie. stronger 3D effects). A subtle difference exists at the very small angles. It was believed to be related to the order of the nonlinearity considered for the least-square fit; however a fifth-order polynomial model did not capture the change in slope at these angles. It may well be due to experimental uncertainties and non-uniformity of the flow in [6] since one would expect a zero moment at zero angle of attack.

Looking now at the right part of Fig. 13, Huang *et al*.'s data appear to be shifted to the left by about half a degree. Otherwise the comparison is good. The fact that all experimental derived curves have a larger slope than the thin airfoil theory curve up to $\theta \approx 3°$ is again attributed to the LSB which has a pitch down effect. Furthermore, the Re = 95,000 and Re = 105,000 moments are very close to each other, and have a larger slope, thus a larger aerodynamic moment stiffness coefficient, than the Re = 77,000 case on the left. This can be related directly to Fig. 5 whereby the pitch oscillation frequency, hence aerodynamic stiffness, is increasing with Reynolds number. Physically, the aft movement of the LSB with Re, as shown in Fig. 9 for $\theta = 0°$ account for this behavior. On the other hand, the thin airfoil theory model does not have any Reynolds number dependency.

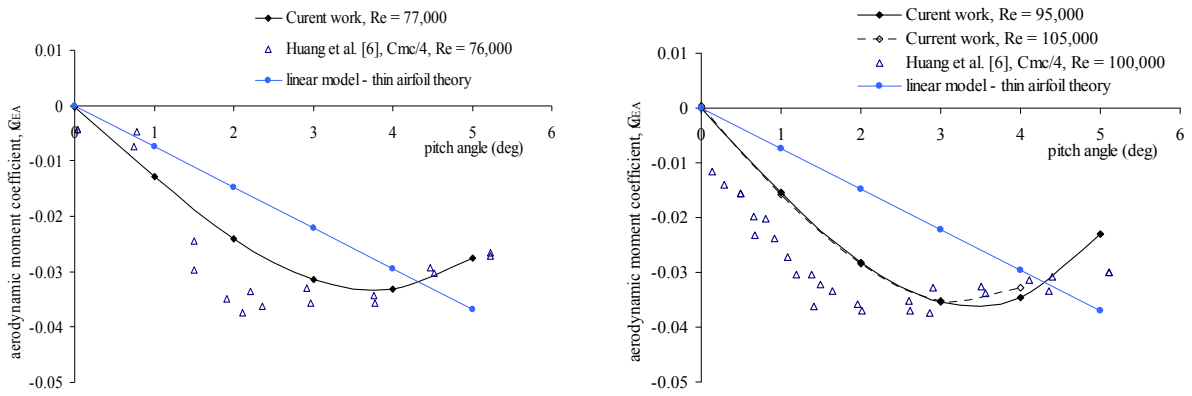


Figure 14 – $C_M(\theta)$; axis at 0.18$c$ for current work and thin airfoil theory, 0.25$c$ for Ref. [6].

Taking a slice in Fig. 12 at a given pitch angle on the aerodynamic moment coefficient – pitch rate plane is relevant to analyze the aerodynamic damping. This is shown in Fig. 15 for $\theta = 0°$ for three different Reynolds numbers. Although no direct results are readily available in the public literature to validate the pitch rate contribution, the aerodynamic moment coefficient as a function of pitch rate, taken at zero pitch angle, makes sense physically. The slope at zero pitch rate is positive which implies a negative aerodynamic damping at these conditions. It represents the wing at the equilibrium point which is dynamically unstable. This is given by the coefficient $a_3$ in Eq. 4. This negative aerodynamic damping is larger in magnitude than the structural damping coefficient, $Ds$, thus resulting in the loss of stability of the equilibrium point with a fluttering behavior. As the oscillations grow and stabilize onto an LCO, the higher order damping terms in Eq. 4, namely $a_8$ and $a_{10}$, become dominant. These terms are negative, hence provide positive aerodynamic damping which counteracts the dynamically de-stabilizing effect of the $a_3$ coefficient.

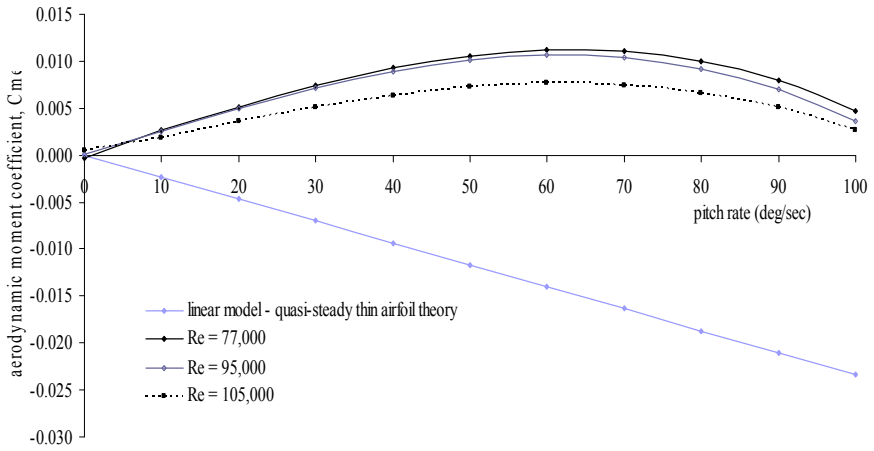


Figure 15 – Aerodynamic moment coefficient as a function of pitch rate, at $\theta = 0°$.
Nominal configuration (EA at 0.18$c$).

## 4.0 CONCLUSION

On the basis of a quasi-steady assumption the aerodynamic moment coefficient of a self-sustained pitching NACA 0012 in the transitional Reynolds number regime has been investigated using the restoring force surface method, in conjunction with a least-square surface fit. To that effect a third-order polynomial in pitch angle and pitch rate, in the sense of a generalized Duffing-van der Pol type nonlinearity, is used. The results are consistent with published data, where available, and are compatible with the observed aeroelastic dynamics. The behavior of the aerodynamic stiffness coefficient is physically explained in terms of the laminar separation and bubble. Flow visualization testing of a static NACA0012 wing at these small angles and transitional Reynolds numbers has provided evidence in support of this claim.

The characteristics of the LCOs are reminiscent of stall flutter, hence dynamic stall, except that they occur at very small pre-stall angles and are strongly Re dependent. The origin of the oscillations is negative aerodynamic damping, and it is speculated that it is also physically related to the laminar trailing edge separation, although no direct evidence is provided at this time. As the oscillations grow onto an LCO, the higher order aerodynamic moment damping terms become stronger and neutralize the dynamically de-stabilizing effect of the linear aerodynamic coefficient. It is speculated as well that these higher order terms are physically related to the LSB and/or the re-attachment point. Preliminary computational aeroelastic simulations using a URANS model have been able to reproduce the self-sustained oscillations [10]. It is expected that these simulations in addition to others based on a LES formulation [11] will provide additional clues on the physical mechanisms leading to, sustaining and then limiting the oscillations.

## 5.0 ACKNOWLEDGEMENTS

The author wishes to acknowledge the work of Xavier Collin who performed the static flow visualization tests within the context of a one-year internship in the Department of Mechanical Engineering at RMC and leading to a Master's from CNAM/SUPAERO, as well as the contribution from Yael Harris who conducted the majority of the aeroelastic testing as part of his research for a Master's at RMC. The financial support of the Department of National Defence, through the ARP and AERAC programs, and the Natural Sciences and Engineering Research Council of Canada (NSERC) are also gratefully acknowledged.

**REFERENCES**

[1] Poirel D., Harris Y. and Benaissa A., Self-sustained aeroelastic oscillations of a NACA0012 airfoil at low-to-moderate Reynolds numbers, Journal of Fluids and Structures. DOI 0.1016/j.jfluidstructs.2007.11.005, 2007.

[2] Gad-el-Hak, M., Control of low-speed airfoil aerodynamics. AIAA Journal 28(9), 1537-1552, 1990.

[3] Mueller, T.J., Low Reynolds number vehicles. AGARD-AG-288, 1985.

[4] Lutz, Th., Würz, W. and Wagner, S., Numerical optimization and wind-tunnel testing of low Reynolds number airfoils. in Fixed and Flapping Wing Aerodynamics for Micro Air Vehicle Applications, edited by T.J. Mueller, Progress in Astronautics and Aeronautics 195, AIAA, Reston, 169-190, 2001.

[5] Mueller, T.J., Aerodynamic measurements at low Reynolds numbers for fixed wing micro-air

vehicles, RTO AVT/VKI Special Course, VKI, Belgium, Sept. 13-17, 1999.

[6] Huang, R.-F., Shy, W.W., Lin, S.W. and Hsiao, F.-B., Influence of surface flow on aerodynamic loads of a cantilever wing. AIAA Journal 34(3), 527-532, 1996.

[7] Huang, R.-F. and Lin, C., Vortex shedding and shear-layer instability of wing at low-Reynolds numbers. AIAA Journal 33(8), 1398-1403, 1995.

[8] Collin, X., Étude de la couche limite du NACA0012 dans un écoulement à faibles nombres de Reynolds, en oscillations libres aéroélastique et à incidences variables, Master's thesis, CNAM/SUPAERO, Oct. 2007.

[9] Worden, K. and Tomlinson, G.R., "Nonlinearity in structural dynamics", Institute of Physics Publishing, London, 2001.

[10] Métivier, V., Dumas, G. and Poirel, D. "Simulations of self-excited pitch oscillations of a NACA 0012 airfoil in the transitional Reynolds number regime", CSME/SCGM, Ottawa, Canada, June 5-8, 2008 (to appear).

[11] Yuan, W., Khalid, M., Poirel, D. and Benaissa, A., "Low-Reynolds-Number Effects on Airfoil Oscillations", 25th AIAA Applied Aerodynamics Conference, Miami, FL, June 25-28, 2007.